

Title: Implications of in-situ chalcogen substitutions in polysulfides for rechargeable batteries

Authors: Sanjay Nanda¹, Amruth Bhargav¹, Zhou Jiang¹, Xunhua Zhao¹, Yuanyue Liu¹, and Arumugam Manthiram^{1*}

Affiliations:

¹Texas Materials Institute, University of Texas at Austin; Austin, TX, 78751, USA.

*Corresponding author. Email: manth@austin.utexas.edu

Abstract: The electrochemical behavior of sulfur-based batteries is governed by polysulfide species. Here, we compare the substitutions of selenium and tellurium into polysulfide chains and their impact on lithium-sulfur battery chemistry. While selenium-substituted polysulfides enhance cathode utilization by effectively catalyzing the sulfur/Li₂S conversion reactions, tellurium-substituted polysulfides improve lithium cycling efficiency by reducing into a passivating interfacial layer on lithium surface with low Li⁺-ion diffusion barriers. This unconventional strategy based on exploiting the intrinsic polysulfide shuttle effect is validated by a ten-fold improvement in the cycle life of lean-electrolyte “anode-free” pouch cells containing no free lithium. The insights generated between the differences of selenium and tellurium chemistries can be applied to benefit a broad range of metal-chalcogen batteries as well as chalcogenide solid electrolytes.

One-Sentence Summary: Polyselenosulfides improve cathode performance, while polytellurosulfides improve anode performance in Li-S batteries

*Corresponding author: Tel: +1-512-471-1791; fax: +1-512-471-7681.
E-mail address: manth@austin.utexas.edu (A. Manthiram)

Main Text: Lithium-sulfur batteries promise significant advantages with respect to energy density, cost, and sustainability as the energy storage landscape transforms in the 21st century (1, 2). The formation of polysulfide (Li_2S_n) species is central to the electrochemistry of Li-S batteries with liquid electrolytes (3, 4). Sulfur demonstrates a strong tendency to catenate and forms reactive polysulfide dianions and radical anions (S_n^{2-} and $\text{S}_{n/2}^{\cdot-}$, $2 < n \leq 8$) that are soluble in a variety of polar protic and aprotic solvents (5, 6). As redox-active intermediates, polysulfides facilitate the sulfur \leftrightarrow Li_2S conversion reaction through a kinetically favored solution-mediated pathway (7–9). The dissolved species also shuttle between the cathode and anode, degrading the lithium surface with insulating $\text{Li}_2\text{S}/\text{Li}_2\text{S}_2$ deposition and compromising cycle life (10–12). The existing challenges with lithium-metal anodes are typically addressed with a fluorinated interface, which may not be compatible with the unique chemistry of the Li-S system (13–15). With the intrinsic constraint of polysulfide species, is there a way to make Li-S batteries practically viable?

Conventional approaches in the literature are primarily focused on suppressing polysulfide dissolution and migration to the lithium anode by modifying the cathode architecture or electrolyte formulation (16–18). In contrast, we show here that polysulfide molecules can be engineered by substituting chalcogen atoms, and the intrinsic shuttle effect can be exploited to enhance electrochemical performance under realistic cell design and testing conditions. We recently reported that a tellurium-rich lithium solid-electrolyte interphase (SEI) enhances the reversibility of lithium deposition (19). In this work, we undertake a comprehensive and comparative study of partially substituting sulfur in the polysulfide chains with its Group 16 counterparts, *viz.*, selenium and tellurium (20). Sharing a similar chemistry with sulfur, Se and Te can be facilely incorporated to form *polyselenosulfides* ($\text{Li}_2\text{Se}_x\text{S}_y$) and *polytellurosulfides* ($\text{Li}_2\text{Te}_x\text{S}_y$) and generated *in-situ* during Li-S cell operation. Variations in the chemical properties of selenium and tellurium lead to significant differences in how they affect the electrochemical performance of Li-S batteries. These differences are systematically delineated in this work, allowing us to formulate a deeper understanding of the electrochemistry of the Li-S system. Employing this unique strategy, we demonstrate lean-electrolyte “anode-free” pouch full cells with high energy density, long cycle life, and zero self-discharge when assembled, thereby moving the Li-S system significantly closer to practical viability. With the insights generated by this work, we expect a similar substitution of selenium and tellurium to have a profound impact on other metal-chalcogen batteries and solid-state batteries employing chalcogenide solid electrolytes.

Results

Molecular Engineering of Polysulfides by Substituting Se and Te

We investigated Se and Te substitution into polysulfides by simply adding 0.06 molar equivalents of elemental Se^0 or Te^0 to 0.1 M Li_2S_6 solution in tetrahydrofuran (THF) and stirring at room temperature for 1 hour. A clear change in color can be observed (Fig. 1A). The yellow-orange polysulfide solution changes to bright red upon reacting with Se and dark brownish red upon reacting with Te.

After filtering out the unreacted residue, the clear solution in the vials was analyzed with liquid chromatography - electrospray ionization - mass spectrometry (LC-EI-MS). A buffer solution of $\text{NH}_4\text{CO}_2\text{CH}_3$ was used as the mobile phase, which protonates the soluble species formed in the reaction between polysulfides and Se/Te (21, 22). Clear signals for $\text{SeS}_2^{\cdot-}$ radical anion and TeS_5^{2-} dianion can be detected as the dominant species in the $[\text{Li}_2\text{S}_6 + \text{Se}]$ and $[\text{Li}_2\text{S}_6 + \text{Te}]$

solutions, respectively (Fig. 1B). They can be positively identified because of the distinctive isotopic signatures of selenium and tellurium (23, 24). Additionally, a range of monosubstituted polysulfides are detected: HSeS_3^- , HTeS_3^- , HSeS_5^- , and TeS_2^- (fig. S1). Thus, the reaction between polysulfides and Se/Te leads to the formation of polyselenosulfides ($\text{Li}_2\text{Se}_x\text{S}_y$) and polytellurosulfides ($\text{Li}_2\text{Te}_x\text{S}_y$), which are realized through a substitution of Se and Te atoms into the polysulfide chain.

To investigate the chemistry of Se and Te substituted polysulfides, the clear solution in the vials was allowed to dry on an inert Si substrate and analyzed with X-ray photoelectron spectroscopy (XPS). Figure 2A shows Se 3d and Te 3d spectra for polyselenosulfide and polytellurosulfide solutions, respectively. A single peak for selenium at ~ 55 eV (corresponding to Se^0) indicates negligible change in oxidation state with the formation of $\text{Li}_2\text{Se}_x\text{S}_y$ species (25). In contrast, a single peak for tellurium at ~ 574.6 eV (intermediate between Te^0 at 573 eV and TeO_2 at 576.3 eV) indicates partial oxidation from Te^0 to $\text{Te}^{+\delta}$ with the formation of $\text{Li}_2\text{Te}_x\text{S}_y$ species (26). This is confirmed with liquid-state nuclear magnetic resonance (NMR) spectroscopy of a polytellurosulfide solution prepared in Acetone- D_6 at -40 °C. Figure 2B shows a clear ^{125}Te peak at +1040 ppm, which is indicative of moderately oxidized Te bonded with electron-withdrawing sulfur atoms (27). Furthermore, quantification of Se 3d and Te 3d and the corresponding S 2p spectra (fig. S2) reveals a large difference in the amounts of selenium and tellurium incorporated into dissolved polyselenosulfide and polytellurosulfide species; 70% and 25% of initially added selenium and tellurium are incorporated, respectively.

To understand these differences, density functional theory was used for calculating the relative energies of substituting one Se or Te atom in Li_2S_6 . Figure 2C shows that it adopts a ring-like configuration, with three independent sites for Se or Te substitution (structures 1 and 6, 2 and 5, 3 and 4 are symmetric). With Se, structures 2 and 3 are energetically favorable with a difference of only 2 meV atom^{-1} , indicating that all four bridging sulfur atoms in Li_2S_6 may be replaced with selenium. With Te, the difference between structures 2 and 3 exceeds 120 meV atom^{-1} , indicating that tellurium has a strong preference for replacing the penultimate sulfur atom. Replacing the terminal sulfur atom is more energetically unfavorable with Te than with Se.

These results show that the substitution of selenium into polysulfides is “quasi-isotopic” (20), on account of the flat energy landscape for different Li_2SeS_5 configurations and negligible change in its oxidation state. In contrast, the substitution of tellurium into polysulfides is less facile, on account of only one Li_2TeS_5 configuration being energetically favorable and accompanying oxidation of Te atoms. The origin of these differences can be ascribed to the relative values of Pauling electronegativity and atomic size for Se (2.55, 115 pm) and Te (2.1, 140 pm) when compared with S (2.58, 100 pm), which is supported by Bader charge analysis of Li_2SeS_5 and Li_2TeS_5 (fig. S3) (28, 29). The contrasting natures of non-polar Se-S and polar Te-S bonds translates into the chemistry and properties of polyselenosulfide and polytellurosulfide molecules.

Application of Se and Te Substituted Polysulfides in Lithium-Sulfur Batteries

In order to understand their effect on the electrochemistry of lithium-sulfur batteries, polyselenosulfide or polytellurosulfide species were generated by simply adding 0.1 molar equivalents of elemental Se^0 and Te^0 (and S^0 as the control) to a Li_2S cathode. $\text{Li}_2\text{Se}_x\text{S}_y$ was formed during cathode preparation, which included a wet ball-milling step, by reaction between Li_2S and 0.1 Se (fig. S4). This is analogous to the formation of Li_2S_n by reaction between Li_2S and 0.1 S and underscores the “quasi-isotopic” nature of Se substitution. A similar reaction was

not observed with tellurium, although $\text{Li}_2\text{Te}_x\text{S}_y$ was formed *in-situ* during cell operation by reaction between polysulfides and 0.1 Te.

Figure 3A shows cyclic voltammograms (CVs) of half cells assembled with $[\text{Li}_2\text{S} + 0.1 \text{ S/Se/Te}]$ cathodes. The presence of polyselenosulfides engenders a significant reduction in peak separation (ΔE_p), indicating diminished overpotentials, and helps retain the canonical redox peaks of sulfur/ Li_2S at high scan rates ($\geq 1 \text{ mV s}^{-1}$). The relationship between peak current (i_p) and scan rate (v) can be written as: $i_p = \alpha v^\beta$, where α and β are fitting parameters (fig. S5) (30). Plotting $\log(i_p)$ versus $\log(v)$ yields $\beta = 0.64$ for Se, compared to 0.52 for the control. An increase in β with the addition of Se indicates a shift away from slow diffusion-controlled reactions and towards fast surface-controlled reactions. The improvement in the redox kinetics is muted more with the introduction of tellurium compared with selenium.

Figure 3B shows the capacities of $\text{Li} \parallel [\text{Li}_2\text{S} + 0.1 \text{ S/Se/Te}]$ half cells at 0.25 A g^{-1} of Li_2S ($\sim \text{C}/5$). It should be noted that while Se is electrochemically active between 2.8 and 1.8 V, Te is inactive in the same voltage window. The addition of 0.1 Se enables a significant enhancement in capacities of $\sim 40\%$ over the control. In contrast, the addition of 0.1 Te brings about no such improvement. The relative dominance of catalytic SeS_2^{\bullet} radical intermediates in polyselenosulfide solutions, as shown in Fig. 1B, facilitates the solution-mediated conversion reactions and drives complete electrochemical utilization (31–33). This is particularly critical for realizing high capacities under lean-electrolyte conditions in a practical Li-S cell (33–35). The presence of highly reactive SeS_2^{\bullet} radicals that may react with various electrolyte components would also explain the faster capacity fade observed after ~ 70 cycles with polyselenosulfides. Conductivity of the sulfur/ Li_2S final products is also improved with the incorporation of Se atoms. Charge/discharge profiles of $\text{Li} \parallel \text{Li}_2\text{S}$ half cells in fig. S6 show that a significant reduction in overpotentials is achieved with selenium compared with sulfur or tellurium (fig. S6). Improvements comparable to those with Se are not realized with a physical mixture of Li_2S and Te as the hindrances to polytellurosulfide formation render a considerable fraction of the added Te inactive in the sulfur/ Li_2S conversion reactions. Therefore, a significant improvement in charge-transfer and redox kinetics is realized with the introduction of selenium but not with tellurium.

Impact of Se and Te Substituted Polysulfides on Lithium Deposition

The migration of dissolved polysulfides from cathode to anode and their reduction to form Li_2S and Li_2S_2 as SEI components is the main factor that renders the dynamics of lithium deposition in Li-S batteries fundamentally unique compared to other systems (36). It stands to reason that Se and Te substituted polysulfides would have a significant impact on lithium interfacial chemistry, and consequently on the dynamics of lithium deposition.

This impact was investigated with anode-free full cells, which contain no excess lithium (N/P ratio = 1) (37, 38), and thereby maximize energy density (39–41). Hence, their electrochemical performance depends entirely on the efficiencies of lithium plating and stripping. Fig. 4A shows capacities for anode-free $\text{Ni} \parallel [\text{Li}_2\text{S} + 0.1 \text{ S/Se/Te}]$ full cells at $\sim 1 \text{ mA cm}^{-2}$ ($\text{C}/5$). Both the control cell and the cell with selenium show rapid capacity fade and lose 50% of their peak capacity within ~ 35 cycles. In sharp contrast, the introduction of tellurium enables remarkable cycling stability in the anode-free configuration and maintains 52% of peak capacity at 265 cycles, when the cell testing was terminated. An average of $\sim 1.8 \text{ mAh cm}^{-2}$ was cycled over this period. The lithium inventory loss rate per cycle is reduced from 2.14% with Se to only 0.24% with Te (42). The Coulombic efficiencies of the anode-free full cells (fig. S7) also reflect this

improvement in lithium plating and stripping reversibility. Thus, the *in-situ* formation of polytellurosulfides has a dramatic effect on lithium cycling efficiencies, despite the kinetic hindrances to tellurium substitution in polysulfides compared with selenium. In contrast, the formation of polyselenosulfides has no effect on the reversibility of lithium deposition.

These improvements were investigated with symmetric Li || Li cells containing $\text{Li}_2\text{Se}_x\text{S}_y$ and $\text{Li}_2\text{Te}_x\text{S}_y$ species introduced ex-situ as electrolyte additives (fig. S8). In contrast to polyselenosulfides, which show high and unstable overpotentials (~ 100 mV), polytellurosulfides enable low and stable overpotentials (~ 10 mV), indicating a thin SEI layer with excellent ionic transport properties. Scanning electron microscopy (SEM) images (fig. S9) show that while lithium cycled with $\text{Li}_2\text{Se}_x\text{S}_y$ is mossy and filamentous, lithium cycled with $\text{Li}_2\text{Te}_x\text{S}_y$ is smooth, planar, and homogenous. The contrasting deposition morphologies help explain the differences in the capacity retention observed in Fig. 4A. The high-surface area non-uniform deposition of lithium with polyselenosulfides leads to the formation of “dead” metallic lithium (43). In contrast, the dense and uniform lithium deposits formed with polytellurosulfides preclude such irreversible loss of lithium inventory.

These results beg the question if a synergetic effect can be achieved with the introduction of both Se and Te. Figure S10 shows the electrochemical performance of an anode-free Ni || Li_2S full cell with 0.05 Se + 0.05 Te additive. It shows that a synergetic effect is indeed realized - higher initial capacities than that with pure 0.1 Te due to the presence of polyselenosulfides and higher cycling stability than that with pure 0.1 Se due to the presence of polytellurosulfides. We believe that the presence of SeS_2^- radicals leads to faster capacity fade with 0.05 Se + 0.05 Te than with 0.1 Te, suggesting that an electrolyte system that stabilizes the radical anion might allow the higher capacities with selenium to be retained over a much longer number of cycles.

These improvements were further validated with practical, large-area ($4.8 \times 8.1 \text{ cm}^2$), single layer pouch cells assembled in the anode-free configuration (N/P = 1) with a 160 mg Li_2S cathode (4.3 mg cm^{-2}) containing 10 wt. % Te^0 (Te : Li_2S molar ratio = 0.04) and operating under lean-electrolyte conditions ($\text{E}/\text{Li}_2\text{S} = 4.5 \text{ } \mu\text{l mg}^{-1}$). In the control, tellurium was replaced by carbon black. As shown in Fig. 4B, the control cell delivered a high initial capacity of 77 mAh but subsequently showed rapid capacity fade and failed (80% retention) within 13 cycles. In contrast, the cell with Te additive exceeded 80% of its peak capacity for nearly 150 cycles and continued cycling without a rapid drop-off in capacity, precluding electrolyte dry-out (44, 45), for over 300 cycles (fig. S11). The ten-fold improvement in cycle life with the introduction of tellurium can be attributed to the stabilizing effect of polytellurosulfides on lithium deposition. The low surface area of plated lithium mitigates parasitic side reactions with the electrolyte, which allows the limited electrolyte supply to be retained over extended cycling. This result validates our strategy under practically relevant cell design and testing parameters. To the best of our knowledge, this is the only reported anode-free pouch cell employing Li_2S cathodes and one of the few reported anode-free pouch cells to date (46, 47). Importantly, this result is achieved with commercial micron-sized Li_2S and Te powder without any optimizations. The anode-free full cell configuration brings about significant practical advantages. It obviates the need to handle or process thin lithium foils, which has proven quite challenging and expensive. Self-discharge, which plagues conventional Li-S cells assembled in the charged state, is eliminated in anode-free full cells that are assembled in the discharged state similar to lithium-ion cells. Achieving long cycle life in the energy-dense, anode-free configuration moves the Li-S system significantly closer to commercial viability.

Impact of Se and Te Substituted Polysulfides on Lithium Interfacial Chemistry

Why is dense, uniform, and reversible lithium deposition without high-surface area mossy growths achieved in the presence of polytellurosulfides, but not in the presence of polyselenosulfides? Much like Li_2S_n , $\text{Li}_2\text{Se}_x\text{S}_y$ and $\text{Li}_2\text{Te}_x\text{S}_y$ species are expected to reduce on the lithium surface and modify the composition of the SEI layer.

In order to understand their effects, the deposited lithium in anode-free full cells after 20 cycles was analyzed with XPS. Figure 5A shows S 2p + Se 3p and Li 1s + Se 3d spectra for the cell with 0.1 Se additive. The S 2p spectra is dominated by oxidized sulfur species (SO_4^{2-}) from LiTFSI decomposition. Analogously, this is also true for the control cell with 0.1 S additive (fig. S12). The Se 3p and Se 3d spectra are dominated by peaks at 165 eV and 58.7 eV, respectively. This corresponds to oxidized Se^{+4} in selenites (SeO_3^{2-}). Reduced sulfur species (Li_2S) are present only as minor components. The presence of oxidized selenium species is due to LiNO_3 , which is a strong oxidizing agent and oxidizes selenides (Se^{2-}) into selenites (SeO_3^{2-}) (48). Thus, the introduction of polyselenosulfides does not fundamentally alter the chemistry of the lithium-electrolyte interface, which remains dominated by oxidized sulfur/selenium species.

Figure 5B shows the S 2p and Te 3d spectra for the cell with 0.1 Te additive. The S 2p spectra is dominated by reduced sulfur species (S^{2-} at 160.6 eV). Likewise, the Te 3d spectra is dominated by sulfidized tellurium species (Te^{+4} at 574.6 eV). Quantification of the spectra reveals the formation of thiotellurate (TeS_3^{2-}) species (19). Thus, polytellurosulfides are reduced on the lithium surface to form Li_2TeS_3 as the dominant interfacial component. In contrast to the previous cases, oxidized sulfur species are now present only as minor components. Furthermore, oxidized tellurium species (TeO_3^{2-}) make up only a minor fraction of tellurium atoms on the lithium surface. Thus, the introduction of tellurium alters the chemistry of the lithium-electrolyte interface towards reduced sulfur species (as Li_2TeS_3) and away from oxidized sulfur species.

The observations made with XPS are validated with time-of-flight secondary ion mass spectrometry (ToF-SIMS). Figure 5C shows the three-dimensional reconstructions of depth profiles for Li_2^- (metallic lithium) and SO_3^- (oxidized sulfur species). A thick layer of electrolyte decomposition products is observed on the deposited lithium with polyselenosulfides but not with polytellurosulfides. Depth profiles in fig. S13 reveal that with selenium, the signal for SeO^- is much stronger compared to SeS^- . This trend is reversed with tellurium, where the signal for TeS^- is much stronger compared to TeO^- . Thus, on the lithium surface, the majority of selenium atoms are bonded with oxygen, while the majority of tellurium atoms are bonded with sulfur. These differences in susceptibility to oxidation by LiNO_3 can be explained by Pearson's HSAB theory (49). Tellurium forms soft Lewis acid cations (Te^{+4}) that prefer soft Lewis bases such as S^{2-} sulfides, while selenium forms hard Lewis acid cations (Se^{+4}) that prefer hard Lewis bases such as O^{2-} oxides (50, 51).

The differences in lithium interfacial chemistry help explain the divergent lithium stabilization capabilities of polyselenosulfides and polytellurosulfides. With interfacial species, a sulfide anionic framework (such as Li_2TeS_3) is preferable compared to an oxide anionic framework (such as Li_2SO_3 or Li_2SeO_3) (52). This is due to the greater size and polarizability of S^{2-} compared to O^{2-} , which reduces Li^+ ion diffusion barriers and improves ionic transport properties. The varying propensities of selenium and tellurium to form a stable sulfide-rich SEI layer in the presence of LiNO_3 additive underlie the observed differences in characteristics of lithium deposition.

Lithium-ion Transport Properties of Selenides, Tellurides, and Thiotellurates

The previous discussion pertained to interfacial components that are present on the surface of the deposited lithium, such as Li_2TeS_3 and Li_2SeO_3 . However, normalized depth profiles for LiTe^- and LiSe^- secondary ions in fig. S14 show that species, such as Li_2Te and Li_2Se , are present throughout the bulk of the porous deposited lithium. In order to understand the impact of these fully reduced species on lithium deposition, their ionic transport properties were evaluated with first-principles calculations.

Li_2S , Li_2Se , and Li_2Te crystallize in a cubic antiferroite structure ($\text{Fm}\bar{3}\text{m}$ space group), with and face-centered cubic anionic framework and Li^+ ions in tetrahedral sites. Li^+ can diffuse along the $[100]$, $[110]$, and $[111]$ directions, as shown in Fig. 6A. The diffusion barriers along each of these pathways was calculated based on the climbing image nudge-elastic-band (CI-NEB) method. The lowest-energy pathway was found to be $[100]$, with calculated barrier energies of ~ 0.3 eV in each case. Along $[110]$ and $[111]$, however, there are significant differences in barrier energies. The transition from Li_2S to Li_2Se to Li_2Te lowers the barrier energy from 0.875 eV to 0.748 eV to 0.539 eV, respectively. This can be explained by the larger size and lower charge density of Te^{2-} , which form a softer and more polarizable anionic framework compared to S^{2-} and Se^{2-} . The larger size of Te^{2-} also lends itself to a more open channel along $[110]$ and $[111]$, which opens additional viable diffusion pathways for Li^+ as shown by a recent work using molecular dynamics simulations (53). With Li_2Te , these alternate pathways facilitate “three-dimensional” ion transport, which enables more uniform, homogenous, and dense lithium deposition.

Li_2TeS_3 crystallizes in a monoclinic structure ($\text{P2}_1/\text{c}$ space group), with trigonal pyramidal TeS_3^{2-} anions arranged in layers and Li^+ ions coordinated to sulfur atoms and occupying alternating tetrahedral and octahedral sites. Eight distinct “steps” between five adjacent and non-equivalent lithium sites in a Li_2TeS_3 unit cell can be identified (fig. S15A), which form part of a complete migration pathway. The single-ion NEB model was applied to approximating the associated barrier energies and identify the most favorable pathway. It corresponds to migration from one tetrahedral site to another tetrahedral site via an intermediate octahedral site along the x-axis, labeled as 2-6-3 (fig. S15B). The migration barriers are 0.378 and 0.250 eV. As shown in Fig. S12b, the barrier energies for other migration pathways lie between 0.4 and 0.6 eV. Hence, there are multiple viable Li^+ ion diffusion pathways in Li_2TeS_3 , which enables “three-dimensional” ionic transport and helps realize stable and reversible lithium deposition. These factors combine to enable a significant improvement in lithium cycling efficiencies with interfacial components formed by the introduction of molecularly engineered polytellurosulfides.

Discussion

Unlocking the promise of lithium-sulfur batteries requires solving two main challenges: increasing energy density with enhanced cathode utilization and improving cycle life by stabilizing the lithium-metal anode. We have shown that both of these challenges can be successfully addressed by the unconventional strategy of engineering polysulfides at the molecular level with selenium and tellurium substitution and exploiting the intrinsic shuttle effect. The practical relevance and effectiveness of this approach is reflected in a 10-fold improvement in cycle life realized in an energy-dense anode-free pouch full cell.

A comparison of the chemical properties of selenium and tellurium and its impact on the electrochemistry of Li-S batteries is profoundly revealing. The quasi-isotopic substitution of selenium and consequent enhancement in charge-transfer and redox kinetics at the cathode suggests that promoting the solid-liquid-solid conversion pathway by stabilizing catalytic

intermediates, such as radical anions, with a suitable electrolyte is a viable strategy towards increasing electrochemical utilization. The shuttle of tellurium-substituted polysulfides to the lithium surface and consequent stabilization of lithium deposition suggests that the *in-situ* formation of a stable ionically conductive sulfide-rich SEI layer is a viable strategy towards improving lithium cycling efficiency. These generalized strategies can potentially be realized by taking advantage of the rich chemistry of ether-soluble catenated sulfur compounds.

These molecularly engineered polysulfides may help solve some of the challenges with alternate metal-sulfur chemistries, such as Na-S and Mg-S batteries, as well as lithium-selenium batteries. The insights generated into the ionic transport properties of different chalcogenides can be useful to the development of superionic sulfide-based solid electrolytes for solid-state batteries. Furthermore, an in-depth understanding of the chemistry of Se and Te substituted polysulfides can find relevance to the development of a wide range of energy materials, including organosulfur compounds, metal complexes with polysulfido ligands, chalcogenide photovoltaics, sulfurized polymers, and layered transition-metal dichalcogenides.

References

1. S. Chung, A. Manthiram, Current Status and Future Prospects of Metal–Sulfur Batteries. *Adv. Mater.* **31**, 1901125 (2019).
2. A. Bhargav, J. He, A. Gupta, A. Manthiram, Lithium-Sulfur Batteries: Attaining the Critical Metrics. *Joule*. **4**, 285–291 (2020).
3. F. Wu, J. T. Lee, N. Nitta, H. Kim, O. Borodin, G. Yushin, Lithium Iodide as a Promising Electrolyte Additive for Lithium-Sulfur Batteries: Mechanisms of Performance Enhancement. *Adv. Mater.* **27**, 101–108 (2015).
4. J. Lei, T. Liu, J. Chen, M. Zheng, Q. Zhang, B. Mao, Q. Dong, Exploring and Understanding the Roles of Li₂Sn and the Strategies to beyond Present Li-S Batteries. *Chem.* **6** (2020), pp. 2533–2557.
5. R. D. Rauh, F. S. Shuker, J. M. Marston, S. B. Brummer, Formation of lithium polysulfides in aprotic media. *J. Inorg. Nucl. Chem.* **39**, 1761–1766 (1977).
6. R. Steudel, T. Chivers, The role of polysulfide dianions and radical anions in the chemical, physical and biological sciences, including sulfur-based batteries. *Chem. Soc. Rev.* **48** (2019), pp. 3279–3319.
7. Y. Son, J. S. Lee, Y. Son, J. H. Jang, J. Cho, Recent Advances in Lithium Sulfide Cathode Materials and Their Use in Lithium Sulfur Batteries. *Adv. Energy Mater.* **5** (2015), , doi:10.1002/aenm.201500110.
8. A. Gupta, A. Bhargav, A. Manthiram, Highly Solvating Electrolytes for Lithium–Sulfur Batteries. *Adv. Energy Mater.* **9**, 1803096 (2019).
9. A. Vizintin, L. Chabanne, E. Tchernychova, I. Arçon, L. Stievano, G. Aquilanti, M. Antonietti, T. P. Fellinger, R. Dominko, The mechanism of Li₂S activation in lithium-sulfur batteries: Can we avoid the polysulfide formation? *J. Power Sources.* **344**, 208–217 (2017).

10. Y. V. Mikhaylik, J. R. Akridge, Polysulfide Shuttle Study in the Li/S Battery System. *J. Electrochem. Soc.* **151**, A1969 (2004).
11. X.-B. Cheng, J.-Q. Huang, Q. Zhang, Review—Li Metal Anode in Working Lithium-Sulfur Batteries. *J. Electrochem. Soc.* **165**, A6058–A6072 (2018).
- 5 12. C. Yan, X. Q. Zhang, J. Q. Huang, Q. Liu, Q. Zhang, Lithium-Anode Protection in Lithium–Sulfur Batteries. *Trends Chem.* **1** (2019), pp. 693–704.
13. J. Xiang, L. Yang, L. Yuan, K. Yuan, Y. Zhang, Y. Huang, J. Lin, F. Pan, Y. Huang, Alkali-Metal Anodes: From Lab to Market. *Joule.* **3** (2019), pp. 2334–2363.
- 10 14. X. Fan, X. Ji, F. Han, J. Yue, J. Chen, L. Chen, T. Deng, J. Jiang, C. Wang, Fluorinated solid electrolyte interphase enables highly reversible solid-state Li metal battery. *Sci. Adv.* **4**, eaau9245 (2018).
- 15 15. S. Liu, X. Ji, J. Yue, S. Hou, P. Wang, C. Cui, J. Chen, B. Shao, J. Li, F. Han, J. Tu, C. Wang, High Interfacial-Energy Interphase Promoting Safe Lithium Metal Batteries. *J. Am. Chem. Soc.* **142**, 2438–2447 (2020).
- 16 16. C. W. Lee, Q. Pang, S. Ha, L. Cheng, S. D. Han, K. R. Zavadil, K. G. Gallagher, L. F. Nazar, M. Balasubramanian, Directing the Lithium-Sulfur Reaction Pathway via Sparingly Solvating Electrolytes for High Energy Density Batteries. *ACS Cent. Sci.* **3**, 605–613 (2017).
- 20 17. C. Zu, N. Azimi, Z. Zhang, A. Manthiram, Insight into lithium-metal anodes in lithium-sulfur batteries with a fluorinated ether electrolyte. *J. Mater. Chem. A*, **3**, 14864–14870 (2015).
18. J. He, A. Manthiram, A review on the status and challenges of electrocatalysts in lithium-sulfur batteries. *Energy Storage Mater.* **20** (2019), pp. 55–70.
- 25 19. S. Nanda, A. Bhargav, A. Manthiram, Anode-free, Lean-Electrolyte Lithium-Sulfur Batteries Enabled by Tellurium-Stabilized Lithium Deposition. *Joule.* **4**, 1121–1135 (2020).
20. F. A. Devillanova, W.-W. Du Mont, *Handbook of chalcogen chemistry: new perspectives in sulfur, selenium and tellurium* (Royal Society of Chemistry, ed. 1, 2013).
- 30 21. J. Gun, A. D. Modestov, A. Kamysny, D. Ryzkov, V. Gitis, A. Goifman, O. Lev, V. Hultsch, T. Grischek, E. Worch, Electrospray ionization mass spectrometric analysis of aqueous polysulfide solutions. *Microchim. Acta.* **146**, 229–237 (2004).
22. A. Bhargav, A. Manthiram, Xanthogen Polysulfides as a New Class of Electrode Material for Rechargeable Batteries. *Adv. Energy Mater.* **10**, 2001658 (2020).
- 35 23. D. C. Lee, A. N. Halliday, Precise determinations of the isotopic compositions and atomic weights of molybdenum, tellurium, tin and tungsten using ICP magnetic sector multiple collector mass spectrometry. *Int. J. Mass Spectrom. Ion Process.* **146–147**, 35–46 (1995).
24. T. M. Johnson, M. J. Herbel, T. D. Bullen, P. T. Zawislanski, Selenium isotope ratios as indicators of selenium sources and oxyanion reduction. *Geochim. Cosmochim. Acta.* **63**, 2775–2783 (1999).
- 40 25. M. Shenasa, S. Sainkar, D. Lichtman, XPS study of some selected selenium compounds. *J. Electron Spectros. Relat. Phenomena.* **40**, 329–337 (1986).

26. M. K. Bahl, R. L. Watson, K. J. Irgolic, X-ray photoemission studies of tellurium and some of its compounds. *J. Chem. Phys.* **66**, 5526–5535 (1977).
27. L. Ronconi, P. J. Sadler, Applications of heteronuclear NMR spectroscopy in biological and medicinal inorganic chemistry. *Coord. Chem. Rev.* **252** (2008), pp. 2239–2277.
- 5 28. J. C. Slater, Atomic radii in crystals. *J. Chem. Phys.* **41**, 3199–3204 (1964).
29. L. R. Murphy, T. L. Meek, A. Louis Allred, L. C. Alien, Evaluation and test of Pauling's electronegativity scale. *J. Phys. Chem. A*. **104**, 5867–5871 (2000).
30. V. Augustyn, J. Come, M. A. Lowe, J. W. Kim, P. L. Taberna, S. H. Tolbert, H. D. Abruña, P. Simon, B. Dunn, High-rate electrochemical energy storage through Li + intercalation pseudocapacitance. *Nat. Mater.* **12**, 518–522 (2013).
- 10 31. M. Cuisinier, C. Hart, M. Balasubramanian, A. Garsuch, L. F. Nazar, Radical or Not Radical: Revisiting Lithium-Sulfur Electrochemistry in Nonaqueous Electrolytes. *Adv. Energy Mater.* **5**, 1401801 (2015).
32. K. H. Wujcik, D. R. Wang, A. Raghunathan, M. Drake, T. A. Pascal, D. Prendergast, N. P. Balsara, Lithium Polysulfide Radical Anions in Ether-Based Solvents. *J. Phys. Chem. C*. **120**, 18403–18410 (2016).
- 15 33. G. Zhang, H. Peng, C. Zhao, X. Chen, L. Zhao, P. Li, J. Huang, Q. Zhang, The Radical Pathway Based on a Lithium-Metal-Compatible High-Dielectric Electrolyte for Lithium–Sulfur Batteries. *Angew. Chemie Int. Ed.* **57**, 16732–16736 (2018).
- 20 34. H. Shin, M. Baek, A. Gupta, K. Char, A. Manthiram, J. W. Choi, Recent Progress in High Donor Electrolytes for Lithium–Sulfur Batteries. *Adv. Energy Mater.* **10**, 2001456 (2020).
35. M. Baek, H. Shin, K. Char, J. W. Choi, New High Donor Electrolyte for Lithium–Sulfur Batteries. *Adv. Mater.* **32**, 2005022 (2020).
- 25 36. S. Nanda, A. Gupta, A. Manthiram, A Lithium–Sulfur Cell Based on Reversible Lithium Deposition from a Li₂S Cathode Host onto a Hostless-Anode Substrate. *Adv. Energy Mater.* **8** (2018), doi:10.1002/aenm.201801556.
37. S. Nanda, A. Gupta, A. Manthiram, Anode-Free Full Cells: A Pathway to High-Energy Density Lithium-Metal Batteries. *Adv. Energy Mater.*, 2000804 (2020).
- 30 38. J. Chen, J. Xiang, X. Chen, L. Yuan, Z. Li, Y. Huang, Li₂S-based anode-free full batteries with modified Cu current collector. *Energy Storage Mater.* **30**, 179–186 (2020).
39. A. A. Assegie, J.-H. Cheng, L.-M. Kuo, W.-N. Su, B.-J. Hwang, Polyethylene oxide film coating enhances lithium cycling efficiency of an anode-free lithium-metal battery. *Nanoscale*. **10**, 6125–6138 (2018).
- 35 40. Z. T. Wondimkun, T. T. Beyene, M. A. Weret, N. A. Sahalie, C. J. Huang, B. Thirumalraj, B. A. Jote, D. Wang, W. N. Su, C. H. Wang, G. Brunklaus, M. Winter, B. J. Hwang, Binder-free ultra-thin graphene oxide as an artificial solid electrolyte interphase for anode-free rechargeable lithium metal batteries. *J. Power Sources*. **450**, 227589 (2020).
41. J. Qian, B. D. Adams, J. Zheng, W. Xu, W. A. Henderson, J. Wang, M. E. Bowden, S. Xu, J. Hu, J.-G. Zhang, Anode-Free Rechargeable Lithium Metal Batteries. *Adv. Funct. Mater.* **26**, 7094–7102 (2016).
- 40 42. S. Nanda, A. Manthiram, Lithium degradation in lithium–sulfur batteries: insights into

inventory depletion and interphasial evolution with cycling. *Energy Environ. Sci.* (2020), doi:10.1039/D0EE01074J.

43. C. Fang, J. Li, M. Zhang, Y. Zhang, F. Yang, J. Z. Lee, M.-H. Lee, J. Alvarado, M. A. Schroeder, Y. Yang, B. Lu, N. Williams, M. Ceja, L. Yang, M. Cai, J. Gu, K. Xu, X. Wang, Y. S. Meng, Quantifying inactive lithium in lithium metal batteries. *Nature*. **572**, 511–515 (2019).
44. X.-B. Cheng, C. Yan, J.-Q. Huang, P. Li, L. Zhu, L. Zhao, Y. Zhang, W. Zhu, S.-T. Yang, Q. Zhang, The gap between long lifespan Li-S coin and pouch cells: The importance of lithium metal anode protection. *Energy Storage Mater.* **6**, 18–25 (2017).
45. S. Chen, C. Niu, H. Lee, Q. Li, L. Yu, W. Xu, J. G. Zhang, E. J. Dufek, M. S. Whittingham, S. Meng, J. Xiao, J. Liu, Critical Parameters for Evaluating Coin Cells and Pouch Cells of Rechargeable Li-Metal Batteries. *Joule*. **3**, 1094–1105 (2019).
46. M. Genovese, A. J. Louli, R. Weber, C. Martin, T. Taskovic, J. R. Dahn, Hot formation for improved low temperature cycling of anode-free lithium metal batteries. *J. Electrochem. Soc.* **166**, A3342–A3347 (2019).
47. A. J. Louli, M. Genovese, R. Weber, S. G. Hames, E. R. Logan, J. R. Dahn, Exploring the impact of mechanical pressure on the performance of anode-free lithium metal cells. *J. Electrochem. Soc.* **166**, A1291–A1299 (2019).
48. L. Zhang, M. Ling, J. Feng, L. Mai, G. Liu, J. Guo, The synergetic interaction between LiNO₃ and lithium polysulfides for suppressing shuttle effect of lithium-sulfur batteries. *Energy Storage Mater.* **11**, 24–29 (2018).
49. R. G. Pearson, Hard and soft acids and bases, HSAB, part I: Fundamental principles. *J. Chem. Educ.* **45** (1968), pp. 581–587.
50. G. Sahu, Z. Lin, J. Li, Z. Liu, N. Dudney, C. Liang, Air-stable, high-conduction solid electrolytes of arsenic-substituted Li₄SnS₄. *Energy Environ. Sci.* **7**, 1053–1058 (2014).
51. Y. Wang, X. Lü, C. Zheng, X. Liu, Z. Chen, W. Yang, J. Lin, F. Huang, Chemistry Design Towards a Stable Sulfide-Based Superionic Conductor Li₄Cu₈Ge₃S₁₂. *Angew. Chemie*. **131**, 7755–7759 (2019).
52. J. Lau, R. H. DeBlock, D. M. Butts, D. S. Ashby, C. S. Choi, B. S. Dunn, Sulfide Solid Electrolytes for Lithium Battery Applications. *Adv. Energy Mater.* **8** (2018), p. 1800933.
53. M. K. Gupta, B. Singh, P. Goel, R. Mittal, S. Rols, S. L. Chaplot, Lithium diffusion in Li₂X (X= O, S, and Se): Ab initio simulations and inelastic neutron scattering measurements. *Phys. Rev. B*. **99**, 224304 (2019).

Acknowledgments: This work used computational resources at National Renewable Energy Lab, the Extreme Science and Engineering Discovery Environment (XSEDE) through allocation TG-CHE190065, and Argonne National Lab. The authors would like to gratefully acknowledge Ian Riddington, Hugo Celio, Andrei Dolocan, Hooman Yaghoobnejad Asl, and Garrett Blake for useful discussions and help with LC-MS, XPS, ToF-SIMS, and NMR data.

Funding:

National Science Foundation award 2011415 (AM)

Welch Foundation award F-1959 (YL)

Author contributions:

Conceptualization: SN, AB, AM

Methodology: SN, AB, ZJ, XZ, AM, YL

5 Investigation (Experimental): SN, AB

Investigation (Computational): ZJ, XZ

Supervision: AM, YL

Writing – original draft: SN, AB, ZJ

Writing – review & editing: SN, AB, ZJ, XZ, AM, YL

10 **Competing interests:** Authors declare that they have no competing interests.

Data and materials availability: All the data generated or analyzed in this study and supporting the conclusions drawn are included in the main article or supporting information. The source data are available from the corresponding author upon reasonable request.

Supplementary Materials

15 Materials and Methods

Figs. S1 to S15

Figures

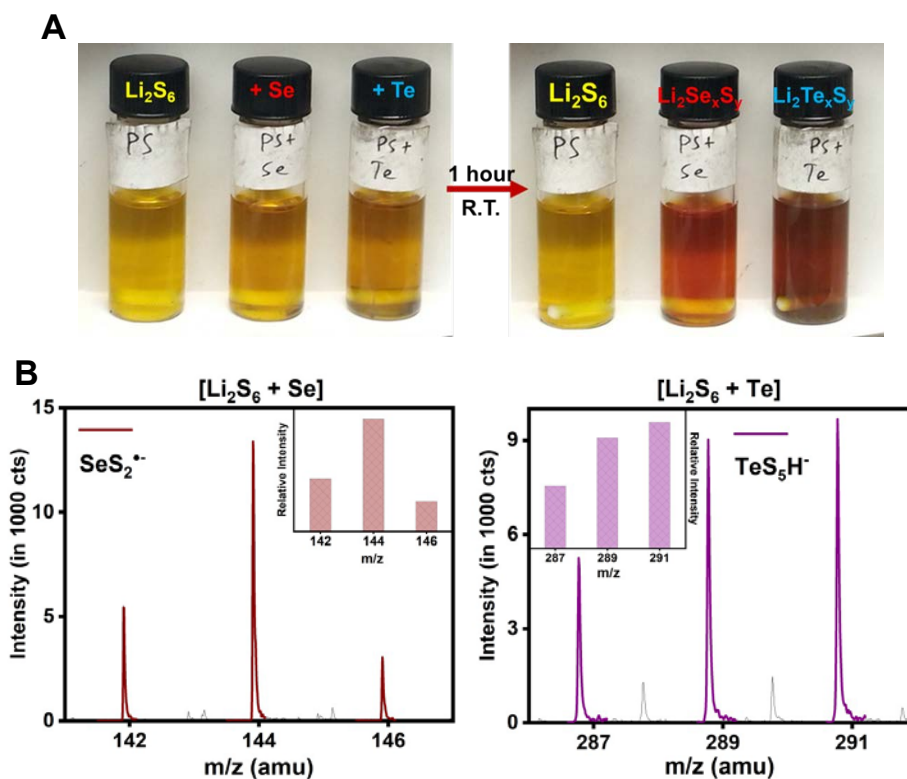


Fig. 1. Incorporation of selenium and tellurium into polysulfide molecules. (A) Photograph of a 0.1 M Li₂S₆ solution in THF reacted with elemental Se⁰ and Te⁰ powder. THF was employed due to its high solubility of polysulfides. A clear change in color can be observed after 1 hour of stirring at room temperature. (B) Mass spectra obtained with LC-MS for [Li₂S₆ + Se] and [Li₂S₆ + Te] solutions indicate the formation of monosubstituted SeS₂^{•-} radical anion and TeS₅²⁻ dianion, which is confirmed by the distinct isotopic signatures of Se and Te. The insets show the relative intensities of the peaks predicted by theory.

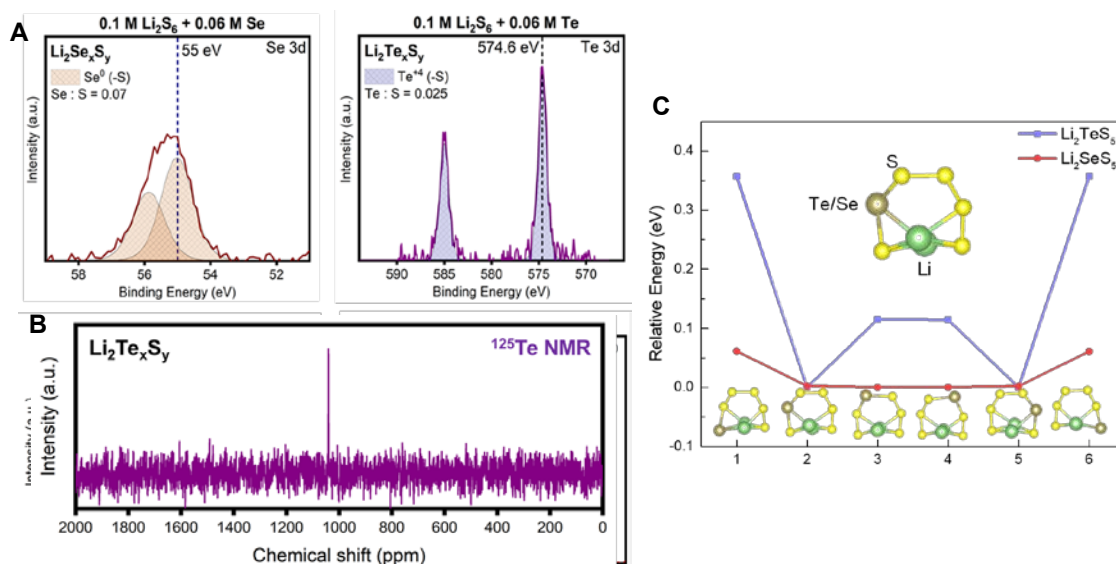


Fig. 2. Chemistry of polyselenosulfides and polytellurosulfides. (A) Se 3d spectra for [Li₂S₆ + Se] solution indicates negligible change in oxidation state of Se. In contrast, the Te 3d spectra for [Li₂S₆ + Te] solution indicates moderate oxidation to Te^{+δ} by the surrounding sulfur atoms. Quantification with S 2p spectra reveals a Se : S ratio of 0.07 and a Te : S ratio of 0.025, indicating that 70% of Se and 25% of Te initially added is dissolved as Li₂Se_xS_y and Li₂Te_xS_y species, respectively. (B) ¹²⁵Te NMR for polytellurosulfides dissolved in D-Acetone at - 40 °C shows a single peak at ~ +1040 ppm, which is typical for inorganic Te (IV) species. (C) Relative energies of six different configurations for the monosubstituted Li₂TeS₅ and Li₂SeS₅ molecules indicates the preference of tellurium for positions 2 and 5 in contrast to the “quasi-isotopic” substitution of selenium.

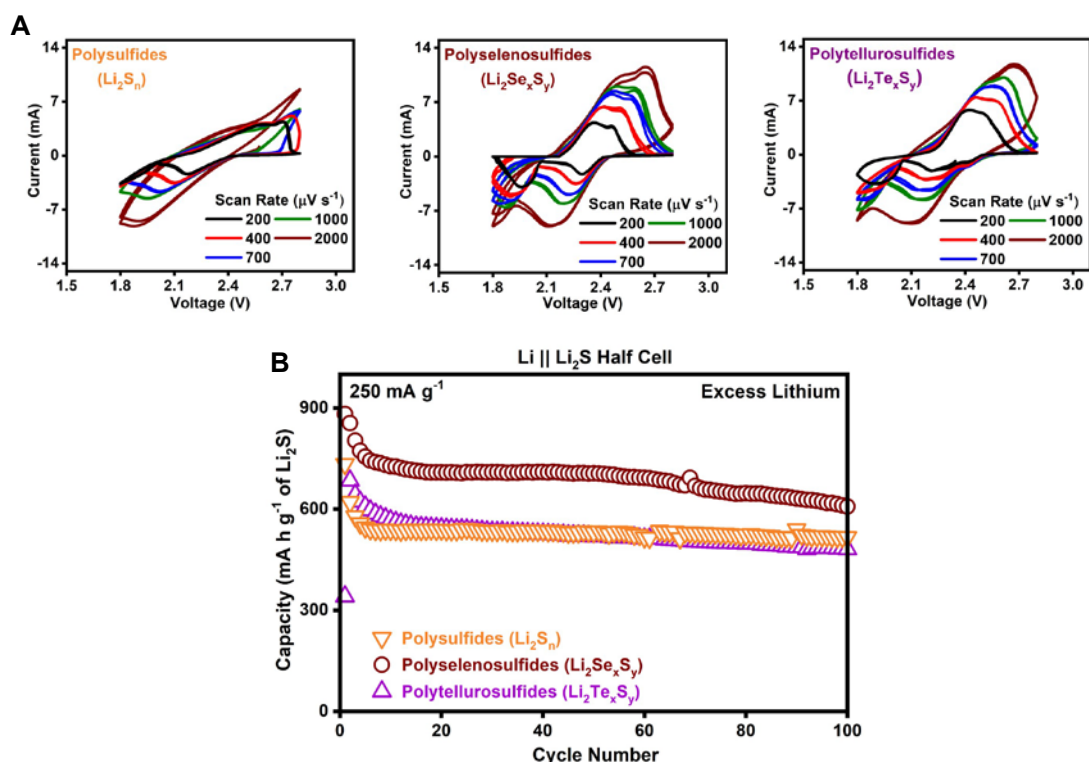


Fig. 3. Impact of polyselenosulfides on redox kinetics and cathode utilization. (A) Cyclic voltammograms for $[\text{Li}_2\text{S} + 0.1 \text{ S/Se/Te}]$ cathodes at scan rates ranging from 200 to $2000 \mu\text{V s}^{-1}$ demonstrate the enhancement in charge-transfer and redox kinetics with the presence of polyselenosulfides. (B) Electrochemical performance of $\text{Li} || [\text{Li}_2\text{S} + 0.1 \text{ S/Se/Te}]$ half cells, which is a function of cathode electrochemical utilization, show that the addition of 0.1 Se enables a $\sim 40\%$ improvement in capacities over the control, while the addition of 0.1 Te has no such effect.

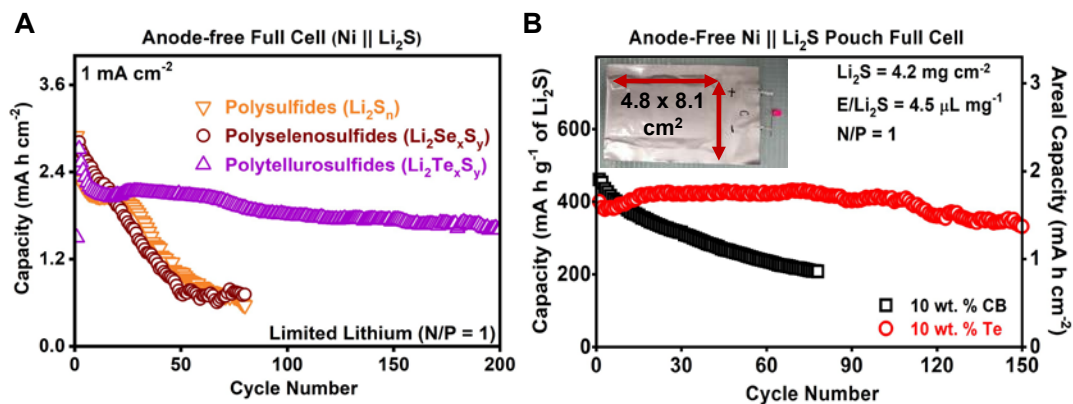


Fig. 4. Impact of polytellurosulfides on lithium anode cycling efficiency. (A) Electrochemical performances of anode-free Ni || [Li₂S + 0.1 S/Se/Te] full cells, describing lithium cycling efficiencies; the data show that in contrast to polysulfides and polyselenosulfides additives, which fail within 40 cycles, polytellurosulfides allow the anode-free full cell to cycle stably for over 250 cycles. (B) Electrochemical performances of large-area (39 cm²) anode-free Ni || Li₂S single-layer pouch full cells with 10 wt. % tellurium (Te : Li₂S molar ratio = 0.04) or 10 wt. % carbon black as cathode additives. The N/P ratio is equal to 1, the E/Li₂S ratio is 4.5 μL mg⁻¹, the Li₂S loading is 4.2 mg cm⁻², and the C-rate is C/10.

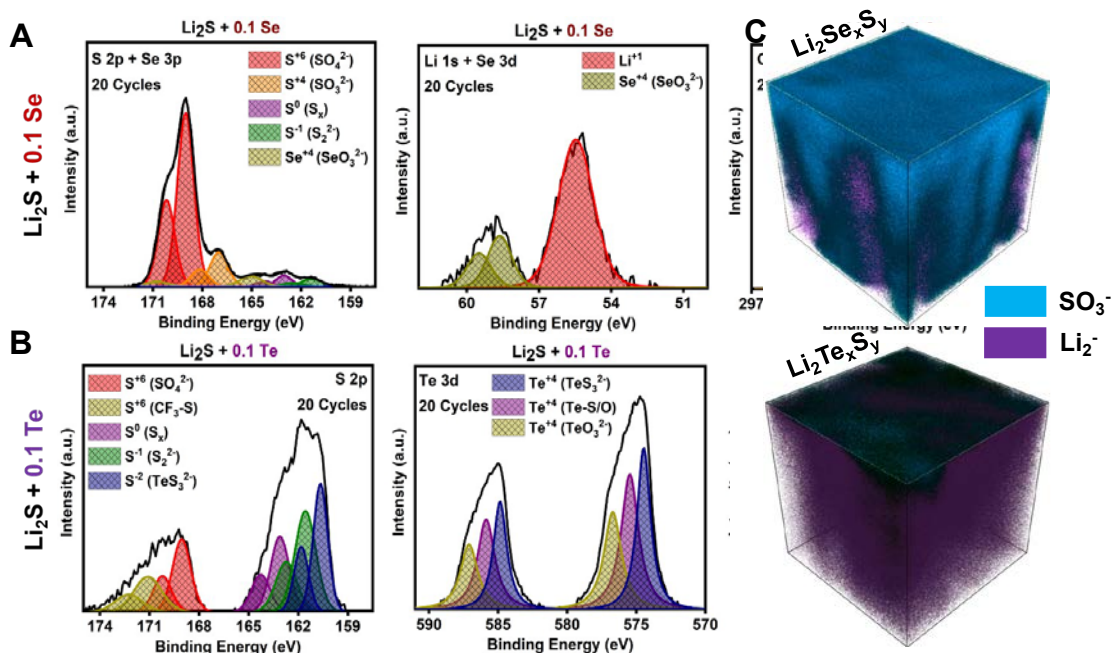


Fig. 5. Interfacial chemistry of lithium surface in the presence of “molecularly engineered” polysulfides. (A) S 2p + Se 3p and Li 1s + Se 3d spectra for the lithium surface in an anode-free full cell cycled with polyselenosulfides. The S 2p spectra is dominated by oxidized sulfur species from electrolyte decomposition, and a peak for oxidized selenium species (Se^{+4} in SeO_3^{2-}) is identified in the Se 3d and Se 3p spectra. (B) S 2p and Te 3d spectra for the lithium surface in an anode-free full cell cycled with polytellurosulfides. Both the Te 3d and S 2p spectra are dominated by thiotellurate (TeS_3^{2-}) species. (C) 3D reconstructions of ToF-SIMS depth profiles for Li_2^- (metallic lithium) and SO_3^- (oxidized sulfur species) secondary ions reveal the differences in the thicknesses of the electrolyte decomposition layer with polyselenosulfides and polytellurosulfides.

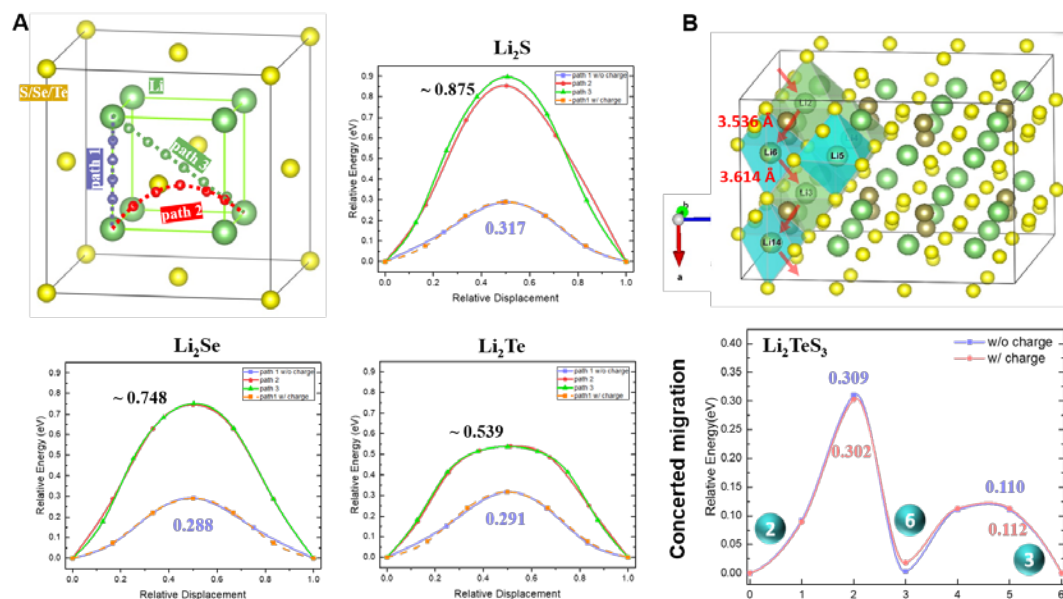


Fig. 6. Ionic transport properties of tellurium-containing interfacial components. (A) Crystal structure of Li_2X ($\text{X} = \text{S}, \text{Se}, \text{and Te}$) and the three Li^+ ion diffusion pathways marked as purple [100], red [110], and green [111] lines. Migration energy barriers along [110] and [111] show a steady reduction from Li_2S to Li_2Se and to Li_2Te . **(B)** Li^+ -ion transport pathway (2-6-3 indicated by red arrows) in Li_2TeS_3 along x-axis and the corresponding energy barrier based on single-ion migration.